Shock Waves
https://doi.org/10.1007/s00193-018-0842-0

ORIGINAL ARTICLE

Hybridized SLAU2–HLLI and hybridized AUSMPW+–HLLI Riemann solvers for accurate, robust, and efficient magnetohydrodynamics (MHD) simulations, part I: one-dimensional MHD

K. Kitamura[1] · **D. S. Balsara**[2]

Received: 21 January 2018 / Revised: 5 June 2018 / Accepted: 8 June 2018

Abstract
SLAU2 and AUSMPW+, both categorized as AUSM-type Riemann solvers, have been extensively developed in gasdynamics. They are based on a splitting of the numerical flux into advected and pressure parts. In this paper, these two Riemann solvers have been extended to magnetohydrodynamics (MHD). The SLAU2 Riemann solver has the favorable attribute that its dissipation for low-speed flows scales as $O(M^2)$, where M is the Mach number. This is the physical scaling required for low-speed flows, and the dissipation in SLAU2 for MHD is engineered to have this low Mach number scaling. The AUSMPW+, when its pressure flux is replaced with that of SLAU2, has the same low Mach number scaling. At higher Mach numbers, however, the pressure-split Riemann solvers were found not to function well for some MHD Riemann problems, despite the fact that they were engineered to have a dissipation that scales as $O(|M|)$ for high Mach number flows. The HLLI Riemann solver (Dumbser and Balsara in J Comput Phys 304:275–319, 2016) has a dissipation that scales as $O(|M|)$, which makes it unsuitable for low Mach number flows. However, it has very favorable performance for higher Mach number MHD flows. Since the two families of Riemann solvers perform very well over a range of intermediate Mach numbers, the best way to benefit from the mutually complementary strengths of both these Riemann solvers is to hybridize between them. The result is an all-speed Riemann solver for MHD. We, therefore, document hybridized SLAU2–HLLI and AUSMPW+–HLLI Riemann solvers. The hybrid Riemann solvers suppress the oscillations that appeared in single-solver solutions, and they also preserve contact discontinuities, as well as Alfvén waves, very well. Furthermore, their better resolution at low speeds has been demonstrated. We also present several stringent one-dimensional test problems.

Keywords SLAU2 · AUSMPW+ · HLLI · MHD · Euler fluxes

1 Introduction

Magnetohydrodynamics (MHD) simulations are crucially important in many areas of science and technology such as astrophysics [1–3], aerospace engineering [4], and nuclear physics [5]. Such simulations are usually carried out with finite-volume codes, and most such codes rely on higher-order Godunov technology. Higher-order Godunov schemes use a higher-order spatial reconstruction, followed by the application of a Riemann solver at zone boundaries to achieve the designed higher-order spatial accuracy. When conjoined with higher-order methods for temporal evolution, such schemes provide a uniformly higher-order solution method. The Riemann solver is an important building block in such methods, and it is our intention in this paper to describe Riemann solvers for MHD that operate well at all speeds.

Riemann solvers for gasdynamics only have to resolve three distinct families of waves in one dimension. For high-speed flow, this is usually accomplished with the use of (flux difference splitting) FDS-based Riemann solvers. Several Riemann solvers that operate successfully for Euler flow have been presented. These include the exact Riemann solver [6,7], the two-shock approximate Riemann

Communicated by H. Luo.

✉ K. Kitamura
kitamura@ynu.ac.jp

D. S. Balsara
dbalsara@nd.edu

[1] Yokohama National University, 79-5 Tokiwadai, Hodogaya-ku, Yokohama, Kanagawa 240-8501, Japan

[2] University of Notre Dame, 225 Nieuwland Science Hall, Notre Dame, IN 46556, USA

Published online: 13 July 2018

solver [8,9], the Roe-type Riemann solver [10,11], the HLL/HLLE/HLLEM Riemann solvers [12–14], the local Lax–Friedrichs (LLF) Riemann solver [15], and the HLLC Riemann solvers [16,17]. It is also worth mentioning the DOT (Dumbser–Osher–Toro) class of universal Riemann solvers [18,19] and the HLLI Riemann solver [20], which is also universal.

For MHD, seven waves appear in the Riemann problem which makes the design of the Riemann solver more intricate. In other words, the MHD system admits fast, Alfvén, and slow waves in both directions in addition to an entropy wave. In MHD, the Roe-type solvers resolve all these waves (7-wave or full-wave) [21–25]. The HLLD Riemann solver of Miyoshi and Kusano [26] only resolves the fast, Alfvén, and entropy waves (5-wave). The HLLC Riemann solver [16,27,28] resolves only the fast waves and the contact discontinuity. Recently, Dumbser and Balsara [20] presented an HLLI Riemann solver which has the potential to be universal and complete. As applied to the MHD system, it can resolve all the waves in the one-dimensional MHD system as long as a complete set of eigenvectors is given.

In gasdynamics, there are many lines of evidence to show that the Roe and HLLC fluxes easily exhibit shock anomalous solutions. In such situations, (flux vector splitting) FVS-based methods seem to work much better. Such methods split the numerical flux into an advected part and a pressure part. Such FVS-based Riemann solvers for gasdynamics include the advection upstream splitting method (AUSM)-type Riemann solver (except for the first AUSM [29]) [30–34] which resolves the sound and entropy waves. There is one overarching reason why FVS-based Riemann solvers are very useful. The reason is that the FDS-based methods have the wrong dissipation characteristics at low Mach numbers [32–37]. To take the Roe-type Riemann solver as an example, at lower Mach numbers, the dissipation continues to scale as $O(|M|)$, where M is the Mach number. However, at low Mach numbers, physical arguments show that the dissipation should scale as $O(M^2)$.[1] It is easy to see that for low Mach numbers, say $|M| \leq 0.1$, the dissipation of the Roe-type Riemann solver would be excessive, resulting in unphysically excessive entropy generation. FVS-based, or pressure-split, Riemann solvers provide more flexibility in their design, permitting this favorable Mach number scaling to be achieved at lower Mach numbers. Another line of evidence shows that the Roe and HLLC fluxes easily exhibit shock anomalous solutions (specifically, Roe and HLLC behave nearly identically [38]), represented by the carbuncle phenomenon [38–40], against which AUSM-type and HLL fluxes are relatively robust. In fact, there is a numerically expressed zone inside the captured shock [34,39–45] where no mathematical expression is valid. In this zone, full-wave solvers tend to pick unphysical waves and augment them—this results in unphysical growth of the carbuncle. In contrast, "less-wave" solvers such as AUSM-type or HLL can suppress such unphysical wave growth and propagation on account of their built-in dissipation. Therefore, several attempts have been made to use a less-wave solver (e.g., HLL) only at a shock and adopt a full-wave flux (e.g., Roe, HLLC) elsewhere [3,46]. SLAU2 [34,38] flux function is one of the AUSM-type solvers and designed to *add a proper amount of dissipation only to the numerical shock zone*. Thus, SLAU2 is robust against shock instabilities, while capable of resolving gasdynamic contacts or boundary layers [34] by itself. Consequently, it can be a good ingredient of a hybrid solver. This is our primary motivation for extending SLAU2 to MHD in this paper. Such an extension would provide the research community with an MHD Riemann solver with correct low Mach number scaling. Consequently, the *first goal* of this paper is to design a SLAU2-based Riemann solver for MHD.

While Roe-type or HLL-type solvers are employed in open astrophysical MHD codes (e.g., [47–51]), there are a very limited number of AUSM-type flux functions for MHD applications, probably because of their lack of Alfvén wave resolution. Only a few FVS-based Riemann solvers for MHD have been presented in the literature. These include E-CUSP [52] and AUSMPW+ [53,54]. While E-CUSP will not accurately capture a stationary contact discontinuity in MHD, AUSMPW+ will capture such a discontinuity. Similarly, SLAU2 can also capture such discontinuities, and this beneficial feature is demonstrated for MHD in this paper. It is also worth pointing out a fine point of difference between SLAU2 and AUSMPW+ in gasdynamic simulations. For gasdynamics, AUSMPW+ is only designed to be a Riemann solver for high-speed flows, whereas SLAU2 is designed to be an all-speed Riemann solver at least in the realm of gasdynamics. Based on extensive testing, we found that within the realm of stringent, high-speed MHD test problems, both SLAU2 and AUSMPW+ Riemann solvers showed some deficiencies. However, they were able performers for low-speed MHD flows.

Several pressure-split solvers have already been improved so that they can simultaneously treat low-speed and high-speed flows accurately. This is often accomplished by hybridizing a pressure-split scheme at lower Mach numbers with a FDS-based Riemann solver at higher Mach numbers. Since FDS-based Riemann solvers can be ruggedized for high Mach number flows, this hybridization offers the best of both worlds—The pressure-split Riemann solver gives favorable low Mach number scaling, while the FDS-based Riemann solver provides robust performance in high Mach

[1] Remember that the pressure coefficient C_p, being $O(1)$, is written as $C_p = 2\Delta p/(\gamma M^2 p_\infty)$, and hence, $\Delta p \propto M^2$. See Appendix A of [55] for more details.

number flows. Such hybrid Riemann solvers are available for gasdynamics where they are sometimes called "all-speed schemes (or Riemann solvers)." In some instances, many user-specified parameters (such as "cutoff Mach number" [32,36]) are required when designing all-speed Riemann solvers. A great deal of attention must be paid to the choice of this cutoff Mach number; otherwise, the solution can be troublesome [32,55,56]. The dissipation term of the SLAU2 Riemann solver for gasdynamics, however, was designed to be automatically scaled to $O(M^2)$ at low speeds, and hence, needs no expert care by the user. We, therefore, realize that if we can hybridize SLAU2 with a FDS-based Riemann solver, we can also offer the best of both worlds for MHD simulations. For our choice of FDS-based Riemann solver, we choose the HLLI Riemann solver [20] because it is a complete Riemann solver that resolves all the waves in the MHD system with a minimum of dissipation for higher Mach number flows. Consequently, the *second goal* of this paper is to document a hybrid SLAU2–HLLI Riemann solver for MHD. This gives us an all-speed Riemann solver for MHD with favorable low Mach number scaling and robust performance at high Mach numbers. In the course of our exploration, we also found that we could redesign the AUSMPW+ Riemann solver for MHD so as to endow it with good low Mach number scaling. This has enabled us to fulfill the *third goal* of this paper which is to document a hybrid AUSMPW+–HLLI Riemann solver for MHD which also has very desirable all-speed capabilities.

To anticipate the utility of all-speed solvers for MHD, let us briefly consider the MHD flows in the Sun as an example. In the solar photosphere, it is not unusual to have convective velocities of $\sim$ 1 km/s with sound speeds of $\sim$ 7 km/s. However, in the solar corona and in the solar wind, velocities can range from 250 to 750 km/s with a sound speed of $\sim$ 100 km/s. A simulation that connects the solar photosphere to the corona would, therefore, have to handle a range of Mach numbers that goes from strongly subsonic to very supersonic. The same simulation, with the same collocation of variables on the mesh, would have to stably straddle this entire range of Mach numbers. This highlights the need for all-speed Riemann solvers for MHD flows. Let us now turn attention to the convective zone in the Sun. At the base of the solar convective zone, convective speeds can be a few km/s, while the sound speed is less than or equal to 200 km/s. In such situations, the anelastic approximation [57–59] has been shown to be deficient [60–62] because it lacks a proper treatment of the energy equation. Even the co-density formulations [63–68] might be deficient in their treatment of energy conservation. In contrast, the full Euler and MHD equations are always energy conservative and it may be worthwhile to ask whether the full equation set, treated explicitly and coupled with an all-speed Riemann solver, might be up to the task? We are not equipped to examine that issue in a computational paper such as this. However, this paper does open the door to a resolution of that question. We point out that in order to examine this issue more thoroughly, we would need a Riemann solver that operates with very low computational cost at low Mach numbers. The SLAU2 Riemann solver is one such very low-cost Riemann solver, whereas the HLLI Riemann solver relies on a characteristic projection and is, therefore, quite computationally costly. For that reason, we design our all-speed Riemann solver in such a way that for flows with a Mach number that is less than 0.1, we revert exclusively to a low-cost SLAU2 Riemann solver for MHD. We hope that this opens the door to treating solar convection with the fully compressible MHD equations rather than cobbled-up equation sets like the anelastic approximation. Furthermore, there are also low Mach flow regions in the International Thermonuclear Experimental Reactor (ITER) according to [69,70].

We confine the present work to one dimension (1D) because multi-dimensional treatments of MHD inevitably call for a divergence-free constraint on the magnetic field ($\nabla \cdot \mathbf{B} = 0$) [71–79]. There are several methods to guarantee this divergence-free property, and the employed method differs from one literature to another (for instance, Han et al. [53] proposed AUSMPW+ for MHD and coupled it with Dedner's method [73], whereas E-CUSP for MHD [52] was developed and tested with a constraint transport method by Balsara and Spicer [72]). In this work, such influences of the choice of divergence treatment method are excluded from our 1D MHD discussion. (The multi-dimensional performance, such as robustness against the carbuncle phenomenon, is deferred to the future work.) Nevertheless, as opposed to gasdynamics, the 1D governing equations for MHD contain multi-dimensional components (y and z components of velocity and magnetic field).

The plan of the paper is as follows. Section 2 describes the governing equations. Section 3 will be dedicated to the discretization of the governing equations, particularly to the SLAU2 and the SLAU2–HLLI in MHD. (AUSMPW+ and AUSMPW+–HLLI in MHD are described in Appendix 1.) Numerical examples will support the performance of the proposed methods on stringent 1D MHD test problems in Sect. 4. Finally, Sect. 5 will conclude the present work.

2 Governing equations

The governing equations are the compressible MHD equations as follows:

$$\frac{\partial \mathbf{Q}}{\partial t} + \frac{\partial \mathbf{F}}{\partial x} + \frac{\partial \mathbf{G}}{\partial y} + \frac{\partial \mathbf{H}}{\partial z} = 0, \tag{1a}$$

$$\mathbf{Q} = \begin{bmatrix} \rho \\ \rho u \\ \rho v \\ \rho w \\ \rho E \\ B_x \\ B_y \\ B_z \end{bmatrix}, \quad \mathbf{F} = \begin{bmatrix} \rho u \\ \rho u^2 + p_{\mathrm{T}} - B_x^2 \\ \rho uv \quad - B_x B_y \\ \rho uw \quad - B_x B_z \\ \rho u H - B_x (\mathbf{u}\cdot\mathbf{B}) \\ 0 \\ u B_y - v B_x \\ u B_z - w B_x \end{bmatrix},$$

$$\mathbf{G} = \begin{bmatrix} \rho v \\ \rho vu \quad - B_y B_x \\ \rho v^2 + p_{\mathrm{T}} - B_y^2 \\ \rho vw \quad - B_y B_z \\ \rho v H - B_y (\mathbf{u}\cdot\mathbf{B}) \\ v B_x - u B_y \\ 0 \\ v B_z - w B_y \end{bmatrix}, \mathbf{H} = \begin{bmatrix} \rho w \\ \rho wu \quad - B_z B_x \\ \rho wv \quad - B_z B_y \\ \rho w^2 + p_{\mathrm{T}} - B_z^2 \\ \rho w H - B_z (\mathbf{u}\cdot\mathbf{B}) \\ w B_x - u B_z \\ w B_y - v B_z \\ 0 \end{bmatrix}, \tag{1b}$$

where $\mathbf{Q}$ is the vector of conservative variables, ρ density, $\mathbf{u} = (u, v, w)^{\mathrm{T}}$ is velocity, p gas pressure, p_{T} total pressure ($p_{\mathrm{T}} = p + B^2/2$), $\mathbf{B}$ magnetic field [$B^2 = \mathbf{B}\cdot\mathbf{B}$; $\mathbf{B} = (B_x, B_y, B_z)^{\mathrm{T}}$], E total energy per unit mass [$E = (p/\rho)/(\gamma - 1) + 0.5(u^2 + v^2 + w^2) + 0.5B^2/\rho$], and H total enthalpy [$H = E + (p/\rho)$]. The working gas is the calorically perfect gas with the specific heat ratio γ. The first five equations are the Euler equations, whereas the 6th–8th equations comprise Faraday's law for MHD, which is a subset of the Maxwell equations.

In 1D, the third and fourth terms are absent, and the 6th equation is dropped. The divergence-free requirement for the magnetic field ($\nabla\cdot\mathbf{B} = 0$) is automatically satisfied, as long as $B_x = $ const. [52]. Then, (1a) is solved with a 1D finite-volume code and can be written in the delta form as:

$$\Delta\mathbf{Q}_i = -\frac{\Delta t}{\Delta x}\left(\mathbf{F}_{i-1/2} - \mathbf{F}_{i+1/2}\right), \tag{2}$$

where $\Delta\mathbf{Q}_i$ is change in conservative variables in time, Δt is the time step, Δx stands for the width of the cell (which is uniform in this study), and $\mathbf{F}_{i\pm1/2}$ is the inviscid (Euler) flux through the cell interface (which separates the cell i and its neighbor cell $i \pm 1$), respectively. Details of the inviscid fluxes are explained below.

3 SLAU2 and SLAU2–HLLI for MHD

3.1 SLAU2 for MHD

Han et al. [53] extended AUSMPW+, one of AUSM-type solvers, and we had first followed their formulation in extending SLAU2 to MHD. However, our preliminary numerical tests demonstrated oscillatory solutions in some cases. We considered that the primary cause of the oscillations lies in the dissipation term (final term) in the mass flux for low speeds, which affects not only the Euler equations (gas flow field) but also the magnetic field governed by the Maxwell equations. In fact, the dissipation term having low Mach scaling was originally developed for gas dynamics, and there is no reason to employ the same dissipation term for the magnetic field. Thus, the following method can be constructed for 1D MHD. Let us begin from the Euler equations part, i.e., the first five components of (1).

$$\mathbf{F}_{\mathrm{SLAU2(Euler)}} = \frac{\dot{m} + |\dot{m}|}{2}\boldsymbol{\Psi}^{+}_{\mathrm{Euler}} + \frac{\dot{m} - |\dot{m}|}{2}\boldsymbol{\Psi}^{-}_{\mathrm{Euler}} + \mathbf{P}_{\mathrm{Euler}} + B_{1/2}\frac{\boldsymbol{\Psi}^{+}_{\mathrm{Euler},B} + \boldsymbol{\Psi}^{-}_{\mathrm{Euler},B}}{2}, \tag{3a}$$

$$\begin{aligned} \boldsymbol{\Psi}^{+}_{\mathrm{Euler}} &= \begin{pmatrix} 1 & u_L & v_L & w_L & H_L \end{pmatrix}^{\mathrm{T}}, \\ \boldsymbol{\Psi}^{-}_{\mathrm{Euler}} &= \begin{pmatrix} 1 & u_R & v_R & w_R & H_R \end{pmatrix}^{\mathrm{T}}, \\ \boldsymbol{\Psi}^{+}_{\mathrm{Euler},B} &= \begin{pmatrix} 0 & -B_{x,L} & -B_{y,L} & -B_{z,L} & 0 \end{pmatrix}^{\mathrm{T}}, \\ \boldsymbol{\Psi}^{-}_{\mathrm{Euler},B} &= \begin{pmatrix} 0 & -B_{x,R} & -B_{y,R} & -B_{z,R} & 0 \end{pmatrix}^{\mathrm{T}}, \end{aligned} \tag{3b}$$

$$\mathbf{P}_{\mathrm{Euler}} = \begin{pmatrix} 0 \\ \tilde{p} \\ 0 \\ 0 \\ \mathrm{P}^{+}\cdot\left\{-u_L B_{x,L} - v_L B_{y,L} - w_L B_{z,L}\right\} B_{1/2} \\ +\mathrm{P}^{-}\cdot\left\{-u_R B_{x,R} - v_R B_{y,R} - w_R B_{z,R}\right\} B_{1/2} \end{pmatrix}, \tag{3c}$$

$$\mathrm{P}^{+} = \begin{cases} \frac{1}{2}\left(1 + \mathrm{sign}\left(M_L\right)\right), & \text{if } |M_L| \geq 1 \\ \frac{1}{4}(M_L + 1)^2\left(2 - M_L\right), & \text{otherwise,} \end{cases} \tag{3d}$$

$$\mathrm{P}^{-} = \begin{cases} \frac{1}{2}\left(1 - \mathrm{sign}\left(M_R\right)\right), & \text{if } |M_R| \geq 1 \\ \frac{1}{4}(M_R - 1)^2\left(2 + M_R\right), & \text{otherwise,} \end{cases} \tag{3e}$$

where $B_{1/2} = \frac{B_{x,L} + B_{x,R}}{2}$ as in [53]. Note that the fifth line of (3c) is proportional to $B_{1/2}$, and hence, it can be included in (3b). For ease of comparison to [53], however, we simply followed their expression here. The mass flux is

$$(\dot{m})_{\mathrm{SLAU2}} = \frac{1}{2}\left\{\rho_L\left(u_L + \left|\bar{V}_n\right|^{+}\right) + \rho_R\left(u_R - \left|\bar{V}_n\right|^{-}\right) - \frac{\chi}{\bar{c}}\left(p_{\mathrm{T},R} - p_{\mathrm{T},L}\right)\right\}, \tag{4a}$$

$$\begin{aligned} |\bar{V}_n|^{+} &= (1 - g)|\bar{V}_n| + g|u_L|, \\ |\bar{V}_n|^{-} &= (1 - g)|\bar{V}_n| + g|u_R|, \end{aligned} \tag{4b}$$

$$\left|\bar{V}_n\right| = \frac{\rho_L\,|u_L| + \rho_R\,|u_R|}{\rho_L + \rho_R}, \tag{4c}$$

$$g = -\max\left[\min\left(M_L, 0\right), -1\right] \times \min\left[\max\left(M_R, 0\right), 1\right] \in [0,\ 1], \tag{4d}$$

where p_{T} is the total pressure ($p_{\mathrm{T}} = p + B^2/2$), and

$$\chi = \left(1 - \hat{M}\right)^2, \tag{4e}$$

$$\hat{M} = \min\left(1.0, \frac{1}{\bar{c}}\sqrt{\frac{\mathbf{u}_L^2 + \mathbf{u}_R^2}{2}}\right), \tag{4f}$$

$$M_L = \frac{u_L}{\bar{c}}, \quad M_R = \frac{u_R}{\bar{c}}, \tag{4g}$$

$$\bar{c} = \frac{c_{f,L} + c_{f,R}}{2}, \tag{4h}$$

where c is, in this MHD case, the fast magnetosonic speed,

$$c_{f,L/R}^2 = \frac{1}{2}\left\{a_{L/R}^2 + \frac{\mathbf{B}_{L/R}^2}{\rho_{L/R}} + \sqrt{\left(a_{L/R}^2 + \frac{\mathbf{B}_{L/R}^2}{\rho_{L/R}}\right)^2 - 4a_{L/R}^2\frac{B_{x,L/R}^2}{\rho_{L/R}}}\right\}, \tag{4i}$$

and $a_{L/R}$ is the gas speed of sound, $a_{L/R}^2 = \frac{\gamma p_{L/R}}{\rho_{L/R}}$.

Then, the pressure flux is:

$$(\tilde{p})_{\mathrm{SLAU2}} = \frac{p_{\mathrm{T},L} + p_{\mathrm{T},R}}{2} + \frac{\mathrm{P}^+ - \mathrm{P}^-}{2}\left(p_{\mathrm{T},L} - p_{\mathrm{T},R}\right) + \sqrt{\frac{\mathbf{u}_L^2 + \mathbf{u}_R^2}{2}}\cdot\left(\mathrm{P}^+ + \mathrm{P}^- - 1\right)\bar{\rho}\bar{c}, \tag{4j}$$

$$\bar{\rho} = \frac{\rho_L + \rho_R}{2}, \tag{4k}$$

for the gasdynamics part [1st–5th lines of (1)]. On the other hand, the magnetic part, i.e., 7th–8th lines (we do not have to solve the 6th line in 1D), is solved by HLL:

$$\mathbf{F}_{\mathrm{SLAU2(Maxwell)}} = \mathbf{F}_{\mathrm{HLL(Maxwell)}} = \frac{S_R\mathbf{F}_L - S_L\mathbf{F}_R + S_L S_R\left(\mathbf{Q}_R - \mathbf{Q}_L\right)}{S_R - S_L}, \tag{5a}$$

$$S_R = \max\left(\hat{u} + c_{f,R},\quad u_R + c_{f,R},\quad 0\right),$$
$$S_L = \min\left(\hat{u} - c_{f,L},\quad u_L - c_{f,L},\quad 0\right), \tag{5b}$$

where $S_{L/R}$ are "signal" speeds traveling in left and right directions, respectively, and $\hat{u}$ is the Roe-averaged [10] velocity,

$$\hat{u} = \frac{\sqrt{\rho_L}u_L + \sqrt{\rho_R}u_R}{\sqrt{\rho_L} + \sqrt{\rho_R}}. \tag{5c}$$

With this simplification of the Faraday's law treatment, the robustness of SLAU2 is dramatically improved. The key idea behind this modification is that we have eliminated the low-Mach-scaled dissipation term from the magnetic part, which would have contaminated the magnetic field.

The idea of separately treating Faraday's law and the Euler equations is not new. Li [28] employed the HLLC flux for the Euler equations while drawing on the HLL flux for the Faraday law, since he found it unstable to use HLLC for both the equations. Our proposal here is in the same spirit, where the Euler equations are solved by SLAU2, whereas HLL is used for the Faraday part.

Notice that the extremal left and right speeds in (5) use the fast speeds. For strongly subsonic flow, this could provide excessive dissipation to the magnetic fields. For low-speed flow situations, we might prefer to use the Alfvén speeds for the dissipation that is imparted to the magnetic fields. Consequently, if we replace the magnetosonic speed, c_{f}, in (5b), with Alfvén speed, c_{A}, we can take Alfvén waves into account and enhance the stability at both shocks and Alfvén discontinuities, according to our preliminary computations.

$$S_{\mathrm{A},R} = \max\left(\hat{u} + c_{\mathrm{A},R}, u_R + c_{\mathrm{A},R}, 0\right),$$
$$S_{\mathrm{A},L} = \min\left(\hat{u} - c_{\mathrm{A},L}, u_L - c_{\mathrm{A},L}, 0\right). \tag{6}$$

The strong shock is detected by the pressure function borrowed from AUSMPW+ flux function (but with c_{A}-weight included) [31,53],

$$w = \min\left(\frac{p_{\mathrm{T},L}}{p_{\mathrm{T},R}}, \frac{p_{\mathrm{T},R}}{p_{\mathrm{T},L}}, \frac{c_{\mathrm{A},L}^2}{c_{\mathrm{A},R}^2}, \frac{c_{\mathrm{A},R}^2}{c_{\mathrm{A},L}^2}\right)^3, \tag{7a}$$

where

$$c_{\mathrm{A},L/R}^2 = \frac{\mathbf{B}_{L/R}^2}{\rho_{L/R}}. \tag{7b}$$

Thus, the following new signal speeds are useful in paying attention to both the fast speed and Alfvén speeds.

$$S_{R,\mathrm{new}} = \max\left((1-w)S_R + wS_{\mathrm{A},R}, 0\right),$$
$$S_{L,\mathrm{new}} = \min\left((1-w)S_L + wS_{\mathrm{A},L}, 0\right), \tag{8}$$

which will be substituted for (5a). The point here is that, when there are no strong shocks in the solution ($w \approx 1$), the flux (for the magnetic field *only*) is soon switched from fast-speed-based HLL (5b) to the Alfvén-speed-based HLL (6), while SLAU2 for the Euler equation part is unaltered. This version will be simply called "SLAU2" in this paper and will be tested in Sect. 5.

We also point out that in the course of development of the present SLAU2 solver, another version is also constructed in which the Maxwell equations are simply treated by a standard AUSM manner, i.e.,

$$\mathbf{F}_{\text{SLAU2(Maxwell)}} = \bar{c}\cdot\left(M^{+}\boldsymbol{\Psi}^{+}_{\text{Maxwell}} + M^{-}\boldsymbol{\Psi}^{-}_{\text{Maxwell}}\right) + \mathbf{P}_{\text{Maxwell}}, \tag{9a}$$

$$\boldsymbol{\Psi}^{+}_{\text{Maxwell}} = \left(B_{y,L}, B_{z,L}\right)^{\text{T}}; \boldsymbol{\Psi}^{-}_{\text{Maxwell}} = \left(B_{y,R}, B_{z,R}\right)^{\text{T}}, \tag{9b}$$

$$\mathbf{P}_{\text{Maxwell}} = \begin{pmatrix} \text{P}^{+}\cdot\{-v_L\}\,B_{1/2} + \text{P}^{-}\cdot\{-v_R\}\,B_{1/2} \\ \text{P}^{+}\cdot\{-w_L\}\,B_{1/2} + \text{P}^{-}\cdot\{-w_R\}\,B_{1/2} \end{pmatrix}, \tag{9c}$$

where

$$M^{+} = \begin{cases} \frac{1}{2}\left(M_L + |M_L|\right), & \text{if } |M_L| \geq 1 \\ \frac{1}{4}\left(M_L + 1\right)^2, & \text{otherwise} \end{cases} \tag{9d}$$

$$M^{-} = \begin{cases} \frac{1}{2}\left(M_R - |M_R|\right), & \text{if } |M_R| \geq 1 \\ -\frac{1}{4}\left(M_R - 1\right)^2, & \text{otherwise} \end{cases} \tag{9e}$$

are commonly used Mach number functions among AUSM-type solvers [30,31]. This version works just as well as the previously proposed version. Consequently, all the numerical results are shown from the previous version of SLAU2.

3.2 Hybrid SLAU2–HLLI for MHD

The HLLI Riemann solver [20] is very briefly reviewed here because such a review makes it easier to explain to the reader how the hybridization takes place between SLAU2 and HLLI Riemann solvers. The HLLI flux is given by taking the HLL flux and adding an anti-diffusive contribution to it, as shown as follows:

$$\mathbf{F}_{\text{HLLI}} = \frac{S_R\mathbf{F}_L - S_L\mathbf{F}_R + S_L S_R\left(\mathbf{Q}_R - \mathbf{Q}_L\right)}{S_R - S_L} - \varphi\frac{S_L S_R}{S_R - S_L}\mathbf{R}_*\left(\overline{\mathbf{Q}}\right)\boldsymbol{\delta}_*\left(\overline{\mathbf{Q}}\right)\mathbf{L}_*\left(\overline{\mathbf{Q}}\right)\left(\mathbf{Q}_R - \mathbf{Q}_L\right), \tag{10a}$$

$$\boldsymbol{\delta}_*\left(\overline{\mathbf{Q}}\right) = \mathbf{I} - \frac{\boldsymbol{\Lambda}^{-}_{*}}{S_L} - \frac{\boldsymbol{\Lambda}^{+}_{*}}{S_R}, \tag{10b}$$

$$\boldsymbol{\Lambda}^{\pm}_{*} = \frac{1}{2}\left(\boldsymbol{\Lambda}_{*} \pm |\boldsymbol{\Lambda}_{*}|\right), \tag{10c}$$

$$\overline{\mathbf{Q}} = \frac{1}{2}\left(\mathbf{Q}_L + \mathbf{Q}_R\right), \tag{10d}$$

where the scalar $\varphi \in [0, 1]$ is a flattener variable (whose detailed definition is deferred to [80]) which responds to the presence of strong shocks (HLL flux for $\varphi = 0$, while HLLI for $\varphi = 1$). In principle, the matrices of right and left eigenvectors, i.e., $\mathbf{R}_*\left(\overline{\mathbf{Q}}\right)$ and $\mathbf{L}_*\left(\overline{\mathbf{Q}}\right)$, can include the entire MHD eigensystem, which yields a complete Riemann solver. However, we are usually only interested in improving the contact discontinuity and Alfven waves. Consequently, $\mathbf{R}_*\left(\overline{\mathbf{Q}}\right)$ and $\mathbf{L}_*\left(\overline{\mathbf{Q}}\right)$ could contain only the linearly degenerate intermediate right and left eigenvectors, and $\boldsymbol{\Lambda}_* = \boldsymbol{\Lambda}_*\left(\overline{\mathbf{Q}}\right)$ is diagonal matrix of eigenvalues, as detailed in [20].

Now a low Mach number scaling can be introduced into the HLLI Riemann solver, with no additional user-specified parameters, as shown in [81]. Remember that we have used the following function χ in SLAU2.

$$\chi = \left(1 - \widehat{M}\right)^2, \tag{4e}$$

$$\widehat{M} = \min\left(1.0, \frac{1}{\bar{c}}\sqrt{\frac{\mathbf{u}_L^2 + \mathbf{u}_R^2}{2}}\right). \tag{4f}$$

Note that $(1-\chi)$ approaches to zero at very low speeds, while it is bounded by unity at supersonic speeds. Furthermore, it needs no cutoff or reference Mach number (velocity), in contrast to the typical preconditioning used in all-speed HLLC [82] or HLLE [83]. Then, with this $(1-\chi)$, the fast and Alfvén speeds are scaled to

$$c_f \to (1-\chi)\,c_f; \quad c_{\text{A}} \to (1-\chi)\,c_{\text{A}}, \tag{11}$$

where $(1-\chi) \approx 2M$ at low speeds. In other words, all the characteristic waves appearing in the Riemann problem are all shrunk to $(1-\chi)$ times their original value. This reduces the dissipation from the HLLI Riemann solver in the low-speed limit.

Keeping this in mind, it is possible to hybridize SLAU2 and HLLI as follows:

$$\mathbf{F}_{\text{SLAU2–HLLI}} = \chi'\mathbf{F}_{\text{SLAU2}} + \left(1-\chi'\right)\mathbf{F}_{\text{HLLI}}, \tag{12a}$$

$$\chi' = \left(1 - \widehat{M}'\right)^2, \tag{12b}$$

$$\widehat{M}' = \min\left(1.0, \max\left(\frac{K}{\bar{c}}\sqrt{\frac{\mathbf{u}_L^2 + \mathbf{u}_R^2}{2}} - \text{M}_{\text{co}}, 0\right)\right), \tag{12c}$$

where $K = 4.0$ is found to be a robust choice (i.e., HLLI is used entirely for $M > 0.25$), and the cutoff number is prescribed as $M_{\text{co}} = 0.1$ so that this solver turns to a full "SLAU2" for $M < 0.1$ (where low-speed flow solvers are favored, such as in the tachocline in the Sun [61,84]). This solver is referred to as "SLAU2–HLLI." Note that χ' (not χ), K, and M_{co} are introduced only for hybridization purposes, and each of the SLAU2 or HLLI Riemann solvers is still parameter-free. Moreover, the same idea will be used in Appendix 1 to construct the ensuing "hybrid AUSMPW+–HLLI Riemann solver."

In this solver, HLLI is usually used at shocks, whereas SLAU2 is employed in low-speed portions of the flow, in this 1D work. In multi-dimensional flows (not covered here,

Table 1 Riemann problems

Problem	ρ	u	v	w	p	B_y	B_z
1: Brio-Wu (left)	1	0	0	0	1	$\sqrt{4\pi}$	0
(right)	0.125	0	0	0	0.1	$-\sqrt{4\pi}$	0
2: Ryu-Jones (left)	1.08	1.2	0.01	0.5	0.95	3.6	2
(right)	1	0	0	0	1	4	2
3: Colliding Flows (left)	0.15	21.55	1	1	0.28	-2	-1
(right)	0.1	-26.45	0	0	0.1	2	1
4: Severe Shock tube (left)	0.8129	1.801	0.3672	0.1836	0.4809	1.7856	0.8928
(right)	1	-1.7942	0	0	0.1	2	1
5: Contact (left)	1	0	0	0	1	0	0
(right)	0.1	0	0	0	1	0	0
6: Alfvén Wave (left)	1/4π	-1	1	-1	1	-1	1
(right)	1/4π	-1	-1	-1	1	1	1

though), however, this will not be the case: Directions perpendicular to the uniform flow or flows inside the boundary layer will more likely adopt SLAU2. Indeed, it is reported that solvers sensitive to characteristic speeds are more vulnerable to carbuncle phenomena in gasdynamics [39,40]. To combat this problem, two different solvers are hybridized in the literature, in which one solver is employed in the shock-normal direction and the other in the shock-perpendicular one (e.g., Roe and HLL for MHD in [3,46], HLLC and HLL in [85], E-CUSP and HLL in [86]). Thus, in future work, the present hybridization will be extended in a multi-dimensional manner against carbuncle phenomena.

4 Numerical tests

An extensive series of 1D test cases were conducted (and seven tests are selected here). We selected these tests because we found that several unhybridized FVS-split solvers successfully handled some problems but failed (diverged, or led to unphysical solution) for the others, as will be demonstrated here. Both the spatial and temporal orders of accuracy are two by explicit second-order TVD [20]. The Courant number is set to as 0.8, unless mentioned otherwise. The computational space of unit length $[-0.5, 0.5]$ is uniformly divided by 400 cells for all the problems. Reference solutions are produced by HLL flux on 4000 cells for the first four cases. Table 1 summarizes Riemann problems from Sects. 4.1–4.7. Solutions of only SLAU2 and SLAU2–HLLI will be presented here, and those of AUSMPW+-type counterparts will be explained in Appendix 1. For ease of comparison, however, the best solver among SLAU2 type and AUSMPW+ type (with its desired condition) in each problem is summarized in Table 2.

4.1 Brio–Wu shock tube

This is a widely used MHD shock tube problem introduced by Brio and Wu [21]. The initial conditions for left (L) and right (R) states are

Problem 1 (Brio–Wu)

$$(\rho, u, v, w, p, B_y, B_z)_L = (1, 0, 0, 0, 1, \sqrt{4\pi}, 0) \quad \text{for } x \le 0,$$
$$(\rho, u, v, w, p, B_y, B_z)_R = (0.125, 0, 0, 0, 0.1, -\sqrt{4\pi}, 0) \quad \text{for } x > 0,$$

Table 2 Best solvers

Problem	Best solvers (desirable condition for such solvers)
1: Brio–Wu	SLAU2, SLAU2–HLLI, AUSMPW+, AUSMPW+–HLLI
2: Ryu–Jones	SLAU2–HLLI, AUSMPW+, AUSMPW+–HLLI
3: Colliding flows	AUSMPW+–HLLI (without low-speed care)
4: Severe shock tube	SLAU2–HLLI, AUSMPW+–HLLI (with full-wave treatment)
5: Contact	SLAU2, SLAU2–HLLI, AUSMPW+, AUSMPW+–HLLI
6: Alfvén wave	SLAU2–HLLI, AUSMPW+–HLLI (with full-wave treatment)
7: Low-speed propagation	SLAU2 (having low-speed care)

with $B_x = 0.75\sqrt{4\pi}$ and $\gamma = 2.0$. Computations are conducted to a final time of $t = 0.1$. The results of SLAU2 are shown in Fig. 1. These results successfully reproduced important physics, such as a (left running) fast rarefaction wave around $x \approx -0.1$, a slow compound wave ($x \approx -0.05$), a contact discontinuity ($x \approx 0.07$), a slow shock at $x \approx 0.15$, and a fast rarefaction wave ($x \approx 0.3-0.36$), as in the reference solution or literature (e.g., HLLI [20]). For this problem, SLAU2–HLLI showed indistinguishable results. For that reason, we do not show the results from the other Riemann solvers.

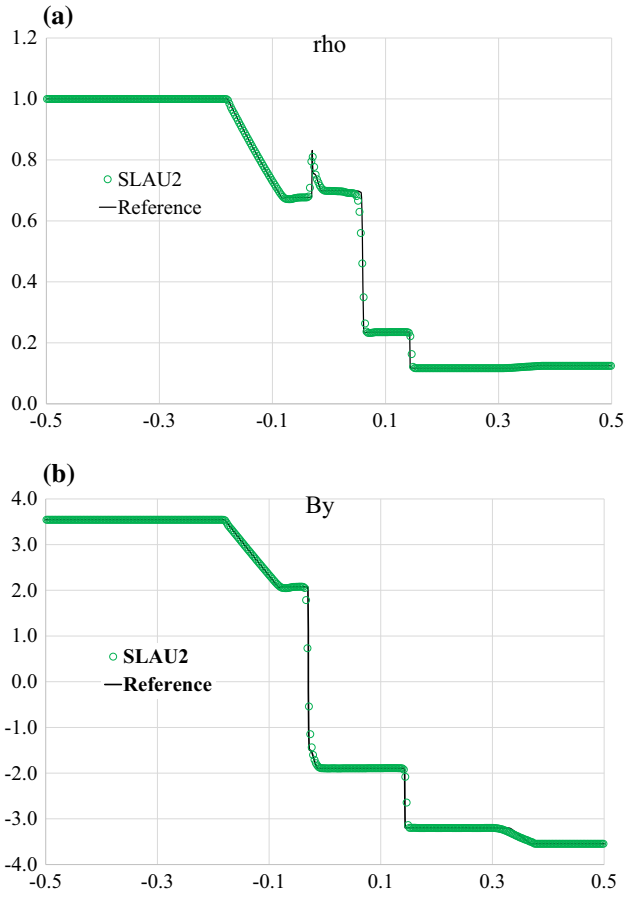

Fig. 1 Problem 1 solutions, SLAU2; **a** density and **b** magnetic field component B_y

4.2 Ryu–Jones shock tube

This problem [22] involves all seven waves, and hence, it is considered to be an important benchmark test case.

Problem 2 (Ryu–Jones)

$$(\rho, u, v, w, p, B_y, B_z)_L = (1.08, 1.2, 0.01, 0.5, 0.95, 3.6, 2) \quad \text{for } x \le 0,$$
$$(\rho, u, v, w, p, B_y, B_z)_R = (1, 0, 0, 0, 1, 4, 2) \quad \text{for } x > 0,$$

with $B_x = 2.0$ and $\gamma = 5/3$. The simulations are run to a final time of $t = 0.2$. The results of SLAU2 are shown in Fig. 2, along with those of SLAU2–HLLI. As seen, all the features are again well captured by SLAU2 as in the reference solution, with only small wiggles observed (Fig. 2, $x \approx -0.2-0$). These oscillations, however, do not appear if SLAU2 is hybridized with HLLI.

4.3 Colliding flows

High-speed flows from both sides collide in this problem [88].

Problem 3 (Colliding)

$$(\rho, u, v, w, p, B_y, B_z)_L = (0.15, 21.55, 1, 1, 0.28, -2, -1) \quad \text{for } x \le 0,$$
$$(\rho, u, v, w, p, B_y, B_z)_R = (0.1, -26.45, 0, 0, 0.1, 2, 1) \quad \text{for } x > 0,$$

with $B_x = 0$ and $\gamma = 5/3$. Computations are conducted for $t = 0.04$. Figure 3 shows the solutions. This is one of the severe problems, and SLAU2 exhibits a density overshoot and oscillations after the shock (Fig. 3, $x \approx -0.3$), as well as in SLAU2-HLLI.

4.4 Severe shock tube problem

In this problem, the following setup is used [88].

Problem 4 (Severe shock tube)

$$(\rho, u, v, w, p, B_y, B_z)_L = (0.8129, 1.801, 0.3672, 0.1836, 0.4809, 1.7856, 0.8928)$$

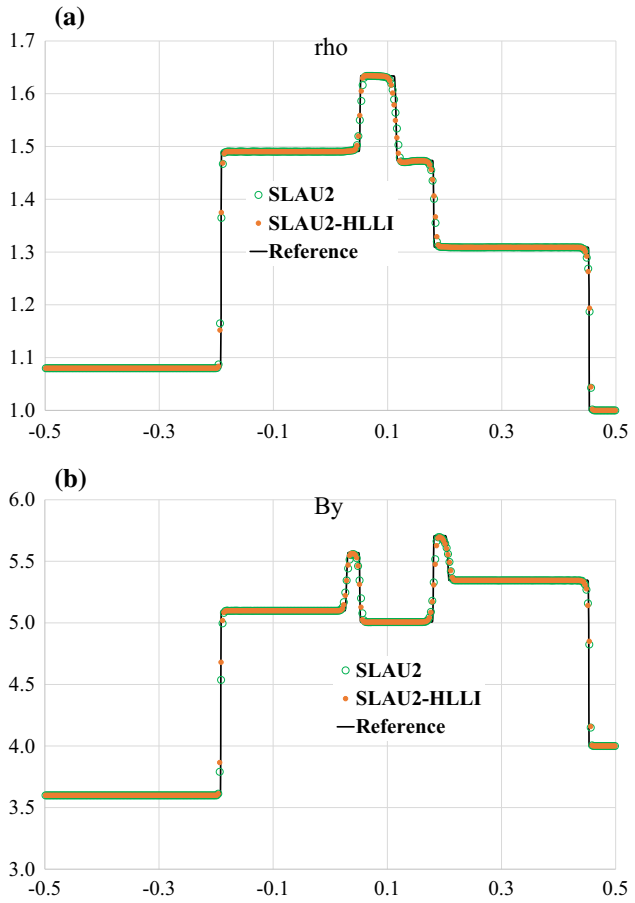

Fig. 2 Problem 2 solutions, SLAU2 and SLAU2–HLLI; **a** density and **b** magnetic field component B_y

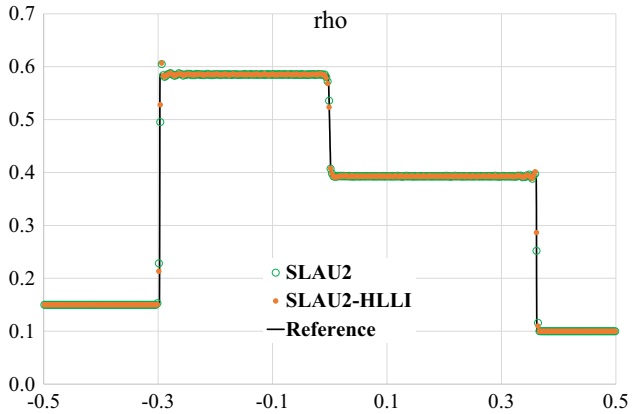

Fig. 3 Problem 3 solutions, density; SLAU2 and SLAU2–HLLI

$$(\rho, u, v, w, p, B_y, B_z)_R = \begin{array}{c} \text{for } x \le 0.1, \\ (1, -1.7942, 0, 0, 0.1, 2, 1) \\ \text{for } x > 0.1, \end{array}$$

with $B_x = 4$ and $\gamma = 5/3$. Computations are conducted for $t = 0.4$. The solutions are shown in Fig. 4 (SLAU2 and SLAU2-HLLI). The magnetic field, B_y, is solved well by all the four solvers (Fig. 4b). In this severe problem, however, the density has unacceptable oscillations at $x \approx 0.1$–0.25 in SLAU2 (Fig. 4a). On the other hand, the oscillations are indeed suppressed in SLAU2–HLLI (Fig. 4a), *demonstrating the benefit of the hybridization*.

4.5 Contact discontinuity

This problem deals with a contact discontinuity.

Problem 5 (Contact discontinuity)

$$(\rho, u, v, w, p, B_y, B_z)_L = (1, 0, 0, 0, 1, 0, 0) \text{ for } x \le 0,$$
$$(\rho, u, v, w, p, B_y, B_z)_R = (0.1, 0, 0, 0, 1, 0, 0) \text{ for } x > 0,$$

with $B_x = 1$ and $\gamma = 1.4$. Computations are conducted for $t = 0.25$. As designed, all the solvers presented here preserve the contact discontinuity (Fig. 5), represented by SLAU2. The exact treatment of isolated contact discontinuities is crucial for achieving well-balanced schemes and is analytically proved for SLAU2 in Appendix 2.

4.6 Alfvén wave discontinuity

In this problem, the following setup is employed.

Problem 6 (Alfvén discontinuity)

$$(\rho, u, v, w, p, B_y, B_z)_L = (1/4\,\pi, -1, 1, -1, 1, -1, 1) \quad \text{for } x \le 0,$$
$$(\rho, u, v, w, p, B_y, B_z)_R = (1/4\,\pi, -1, -1, -1, 1, 1, 1) \quad \text{for } x > 0,$$

with $B_x = 1$ and $\gamma = 1.4$. Computations are conducted for $t = 0.25$. The solutions are shown in Fig. 6. As seen, the SLAU2 smeared out the stationary Alfvén discontinuity, obviously because of lack of Alfvén wave resolution. The SLAU2–HLLI, on the other hand, perfectly preserves the sharp jump in magnetic variables. Thus, *the importance of hybridizing with the HLLI full-wave solver has been confirmed*.

4.7 Low-speed wave propagation

This final test case is not a Riemann problem, but useful in assessing the performance of Riemann solvers at low speeds in 1D. Here, the initial linear variations for pressure are given by following equations from [89,90].

Problem 7 (Low speed)

$$p_i' = \varepsilon\, p_0 \sin(2\pi x/n),$$

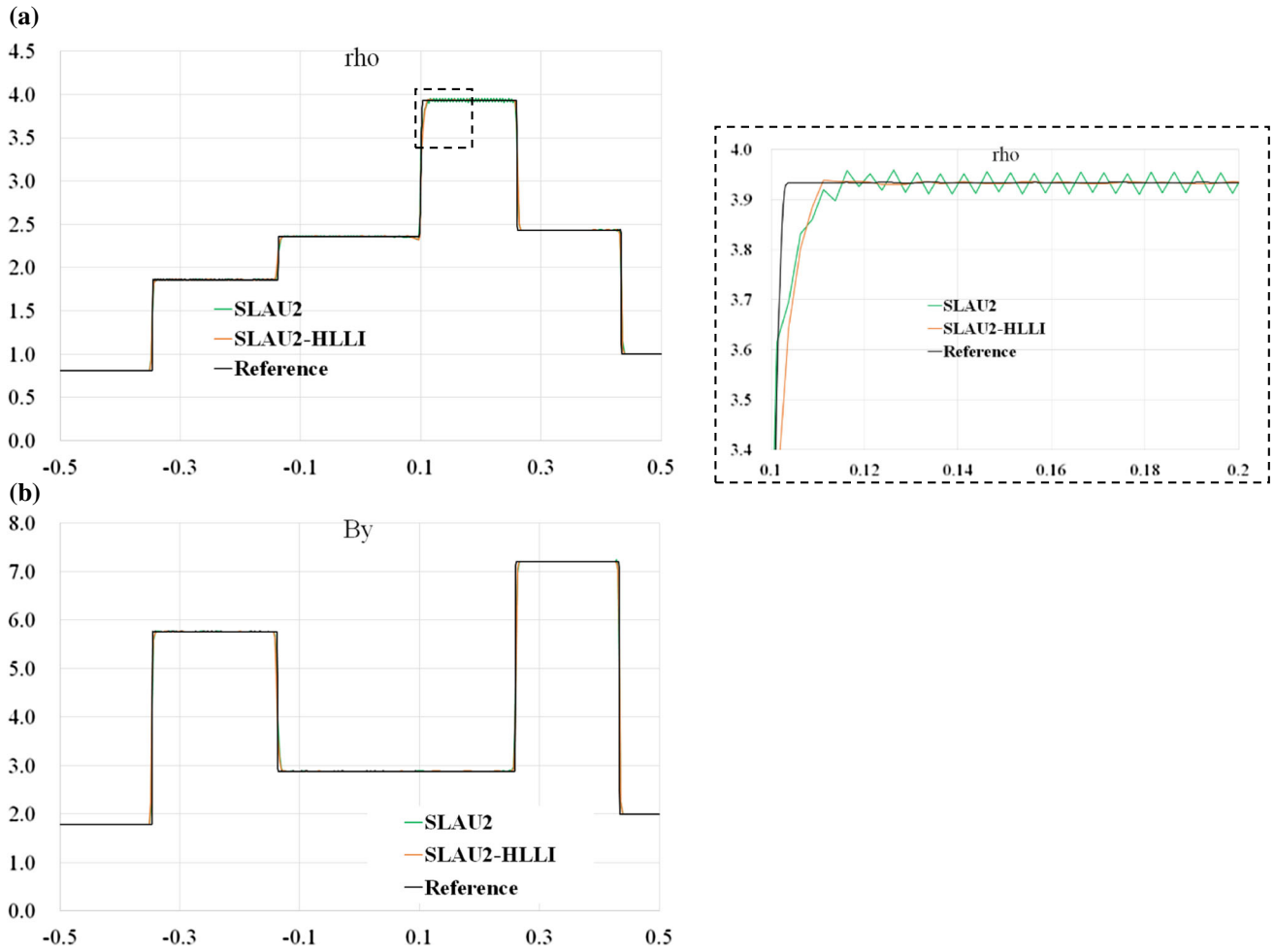

Fig. 4 Problem 4 solutions, SLAU2 and SLAU2–HLLI; **a** density and **b** magnetic field component B_y

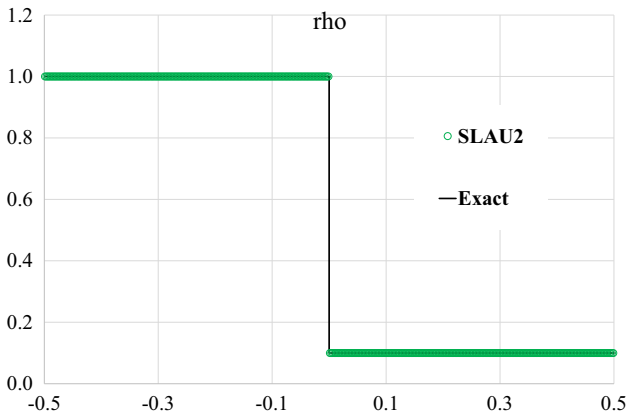

Fig. 5 Problem 5 solutions, density; SLAU2

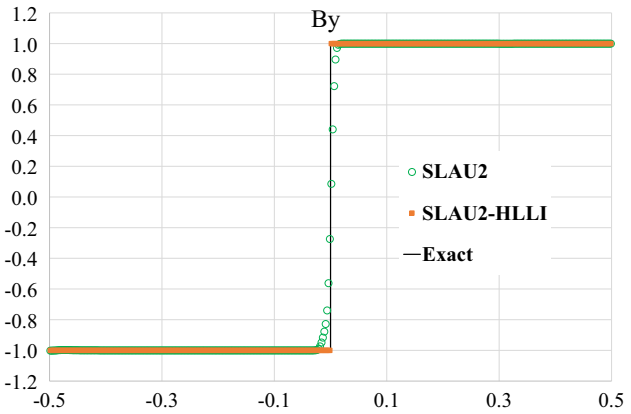

Fig. 6 Problem 6 solutions, magnetic field component B_y; SLAU2 and SLAU2–HLLI

where $B_x = 0.001$, background pressure p_0 and density being 1, and background velocity being 0.1. Here, one wavelength $\lambda(= 0.05)$ is composed of $n = 20$ cells, and ε is a small number 0.001, which stands for the magnitude of pressure variation from the mean value.

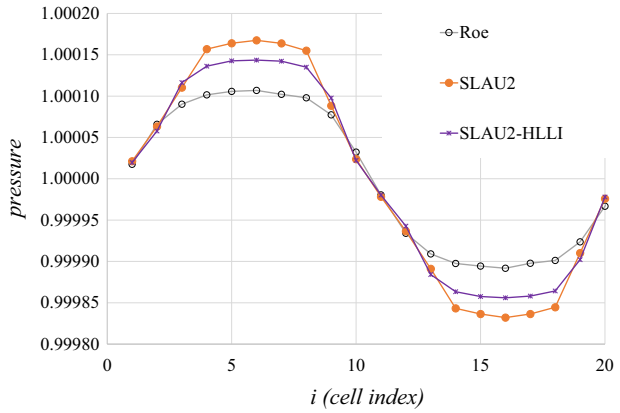

Fig. 7 Problem 7 solutions

Figure 7 shows the pressure profiles in the first 20 cells at $t = 1$ of the present problem. As time progresses, the wave amplitude is known to decay. SLAU2, nevertheless, attained the highest amplitude (17%), followed by SLAU2–HLLI (14%). The Roe-type Riemann solver showed the smallest amplitude (11%) which has no low Mach scaling, for reference.

Note that in steady multi-dimensional problems, these differences will result in huge discrepancies from physically valid solutions, as is evident in Appendix 3 or [33,35] (especially Fig. 13 in [33], in which SLAU preserved the initial shape of a Rankine vortex very well whereas it had decayed by Roe solution after long time computations). This will be thoroughly covered in our next paper. In this 1D context, however, the present problem may be the best way to demonstrate the effects of low-speed scaling introduced in SLAU2 and SLAU2–HLLI, although it is considered a test for Euler equations without the magnetic field.

5 Conclusions

SLAU2, categorized as an AUSM-type Riemann solver, has been extended to magnetohydrodynamics (MHD). SLAU2 is equipped with a proper dissipation term for both high speed and low speed flows. AUSMPW+, having no such term, has also been suitably upgraded by using the dissipation term from SLAU2. Despite their robust performance in gasdynamics at super- and hypersonic speeds, these solvers were found not to function well for MHD problems under extreme conditions. While the SLAU2 and AUSMPW+ Riemann solvers for MHD were able to solve several typical benchmark cases, in a few severe, high Mach tests, they failed to obtain stable solutions.

The HLLI Riemann solver, on the other hand, was not designed for low Mach number flows. However, it has very favorable performance for higher Mach number MHD flows. Since the two families of Riemann solvers perform very well over a range of intermediate Mach numbers, we decided to hybridize between them, to obtain an all-speed Riemann solver for MHD. That is, we proposed hybridized SLAU2–HLLI and AUSMPW+–HLLI Riemann solvers. The hybrid Riemann solvers suppressed the oscillations that had appeared in single-solver solutions, and they also preserved contact discontinuities, as well as Alfvén waves, very well. Furthermore, their better resolution at low speeds has been demonstrated.

We presented several stringent one-dimensional test problems. The multi-dimensional extension is definitely the next step and will appear as a future work.

Acknowledgements This work has been conducted while the first author (K. Kitamura) was visiting at the University of Notre Dame. We would like to express gratitude to the University of Notre Dame for hosting the first author and also to Yokohama National University for financial support. The first author also thanks Shigenobu Hirose and Takashi Minoshima at JAMSTEC (Japan Agency for Marine-Earth Science and Technology), Japan (introduced through Eiji Shima, JAXA), and Nishant M. Narechania at University of Toronto, Canada, and Dan Hori at Nagoya University, Japan, for providing him with fundamental knowledge on astrophysics and nuclear fusion, respectively. Last but not least, he really appreciates Meng-Sing Liou at NASA Glenn Research Center for his continuous discussions on SLAU2, one of AUSM-family fluxes. The second author (DSB) acknowledges support via NSF Grants NSF-DMS-1361197, NSF-ACI-1533850, NSF-DMS-1622457, and NSF-ACI-1713765. Several simulations were performed on a cluster at UND that is run by the Center for Research Computing. Computer support on NSF's XSEDE and Blue Waters computing resources is also acknowledged.

Appendices

Appendix 1: AUSMPW+, AUSMPW+–HLLI, AUSMPW+2, and AUSMPW+2–HLLI for MHD

The AUSMPW+ flux was already extended to MHD by Han et al. [53]. This form, however, turned out to be unstable in some numerical tests, as was the case with the original SLAU2. Thus, it is modified, as in SLAU2, in which the gasdynamic part and magnetic part are handled differently, as follows. The Euler part is

$$\mathbf{F}_{\mathrm{AUSMPW+(Euler)}} = \bar{M}_L^{+} c_{1/2} \mathbf{\Phi}_L + \bar{M}_R^{-} c_{1/2} \mathbf{\Phi}_R + \mathrm{P}^{+}\mathbf{P}_L + \mathrm{P}^{-}\mathbf{P}_R + \frac{1}{2}\left(\mathbf{F}_{\mathrm{B},L} + \mathbf{F}_{\mathrm{B},R}\right), \tag{13a}$$

$$\mathbf{\Phi} = \left(\rho, \rho u, \rho v, \rho w, \rho E + p_{\mathrm{T}}\right)^{\mathrm{T}},$$
$$\mathbf{F}_{\mathrm{B}} = \left(0, -B_{1/2}B_x, -B_{1/2}B_y, -B_{1/2}B_z, 0\right)^{\mathrm{T}}, \tag{13b}$$
$$\mathbf{P} = \left(0, p_{\mathrm{T}}, 0, 0, -B_{1/2}\left(\mathbf{u}\cdot\mathbf{B}\right)\right)^{\mathrm{T}}, \tag{13c}$$

where $B_{1/2} = \frac{B_{x,L}+B_{x,R}}{2}$ as in [53], and for $m_{1/2} = \overline{M}_L^+ + \overline{M}_R^- \geq 0$,

$$\begin{aligned}\overline{M}_L^+ &= M_L^+ + M_R^- \cdot [(1-w)\cdot(1+f_R) - f_L]\,,\\ \overline{M}_R^- &= M_R^- \cdot w \cdot (1+f_R)\,,\end{aligned} \tag{14a}$$

and for $m_{1/2} < 0$,

$$\begin{aligned}\overline{M}_L^+ &= M_L^+ \cdot w \cdot (1+f_L)\,,\\ \overline{M}_R^- &= M_R^- + M_L^+ \cdot [(1-w)\cdot(1+f_L) - f_R]\,.\end{aligned} \tag{14b}$$

The pressure-based weighting functions are given by:

$$w = 1 - \min\left(\frac{p_{\mathrm{T},L}}{p_{\mathrm{T},R}}, \frac{p_{\mathrm{T},R}}{p_{\mathrm{T},L}}\right)^3, \tag{14c}$$

$$f_{L/R} = \begin{cases} \left(\frac{p_{L/R}}{p_{\mathrm{T},s}} - 1\right), & \text{if } p_{\mathrm{T},s} \neq 0,\\ 0, & \text{if } p_{\mathrm{T},s} = 0,\end{cases} \tag{14d}$$

$$p_{\mathrm{T},s} = \mathrm{P}^+ p_{\mathrm{T},L} + \mathrm{P}^- p_{\mathrm{T},R}, \tag{14e}$$

where the pressure flux, which was not given in [53] or [54], is assumed as the standard AUSM form as (3d) and (3e) (that drops off higher-order terms):

$$\mathrm{P}^+ = \begin{cases} \frac{1}{2}\left(1 + \mathrm{sign}\,(M_L)\right), & \text{if } |M_L| \geq 1\\ \frac{1}{4}(M_L+1)^2\,(2 - M_L)\,, & \text{otherwise,}\end{cases} \tag{3d}$$

$$\mathrm{P}^- = \begin{cases} \frac{1}{2}\left(1 - \mathrm{sign}\,(M_R)\right), & \text{if } |M_R| \geq 1\\ \frac{1}{4}(M_R-1)^2\,(2 + M_R)\,, & \text{otherwise,}\end{cases} \tag{3e}$$

and the mass flux switch, again not given in [53] or [54], is assumed as follows (again dropping off higher-order terms):

$$M^+ = \begin{cases} \frac{1}{2}\left(M_L + |M_L|\right), & \text{if } |M_L| \geq 1\\ \frac{1}{4}\,(M_L+1)^2\,, & \text{otherwise,}\end{cases} \tag{9d}$$

$$M^- = \begin{cases} \frac{1}{2}\left(M_R - |M_R|\right), & \text{if } |M_R| \geq 1\\ -\frac{1}{4}\,(M_R-1)^2\,, & \text{otherwise,}\end{cases} \tag{9e}$$

where

$$M_L = \frac{u_L}{\bar{c}}, \quad M_R = \frac{u_R}{\bar{c}}, \tag{15a}$$

$$\bar{c} = \min\left(c_{f,L},\, c_{f,R}\right), \tag{15b}$$

that is, the minimum value of the left and the right c (fast magnetosonic speed) is taken.

The magnetic part is common to SLAU2 for MHD and hence omitted. Also, as in SLAU2, another version has also been developed which does not use HLL but a simple AUSM form in the magnetic part, and this works well as in the present AUSMPW+. The solutions are not shown. Furthermore, the same idea as in Sect. 3.2 will lead to "AUSMPW+–HLLI."

The selected numerical results are shown in Fig. 8 for Problem 3 (Colliding Flow). In this problem, in contrast to SLAU2 and SLAU2–HLLI (Fig. 3), AUSMPW+ produces only small wiggles and very slight undershoot ($x \approx -0.0$) that are similar in AUSMPW+–HLLI (Fig. 8). For this particular high-speed test, AUSMPW+ suppressed wiggles in SLAU2 which is designed for both high and low speeds. For the other problems, SLAU2 represents AUSMPW+, and SLAU2–HLLI does AUSMPW+–HLLI, respectively, except for Problem 2 (Ryu–Jones shock tube) in which SLAU2–HLLI, AUSMPW+, and AUSMPW+–HLLI removed small wiggles seen in SLAU2.

Furthermore, since AUSMPW+ does not have a low-speed scaling term, we replaced its pressure flux with that of the SLAU2, leading to "AUSMPW+2" and "AUSMPW+2–HLLI" as follows:

$$\begin{aligned}\mathbf{F}_{\mathrm{AUSMPW+2(Euler)}} = {}& \overline{M}_L^+ c_{1/2}\boldsymbol{\Phi}_L + \overline{M}_R^- c_{1/2}\boldsymbol{\Phi}_R\\ &+ \mathbf{P}_{\mathrm{AUSMPW+2}} + \frac{1}{2}\left(\mathbf{F}_{\mathrm{B},L} + \mathbf{F}_{\mathrm{B},R}\right),\end{aligned} \tag{16a}$$

$$\mathbf{P}_{\mathrm{AUSMPW+2}} = \begin{pmatrix} 0\\ \tilde{p}\\ 0\\ 0\\ \mathrm{P}^+\cdot\left\{-u_L B_{x,L} - v_L B_{y,L} - w_L B_{z,L}\right\} B_{1/2}\\ +\mathrm{P}^-\cdot\left\{-u_R B_{x,R} - v_R B_{y,R} - w_R B_{z,R}\right\} B_{1/2}\end{pmatrix}, \tag{16b}$$

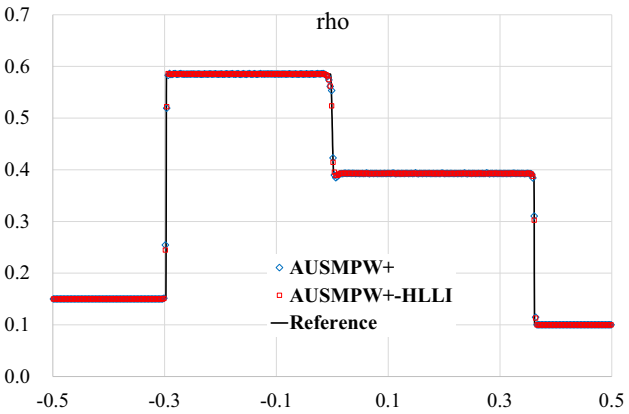

Fig. 8 Problem 3 solutions, density; AUSMPW+ and AUSMPW+–HLLI

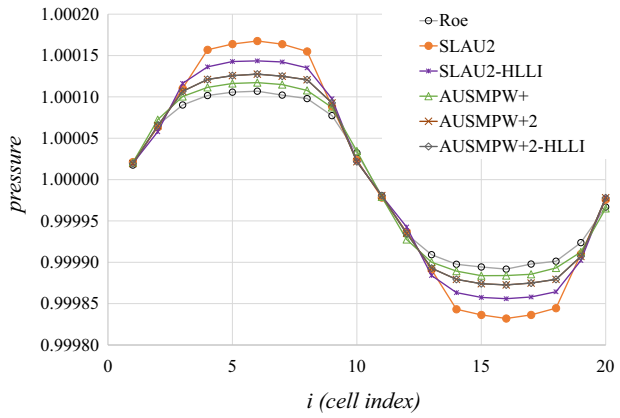

Fig. 9 Problem 7 solutions (including AUSMPW+2 and AUSMPW+2–HLLI)

where

$$(\tilde{p})_{\mathrm{AUSMPW+2}} = (\tilde{p})_{\mathrm{SLAU2}} = \frac{p_{\mathrm{T},L} + p_{\mathrm{T},R}}{2} + \frac{\mathrm{P}^+ - \mathrm{P}^-}{2}\left(p_{\mathrm{T},L} - p_{\mathrm{T},R}\right) + \sqrt{\frac{\mathbf{u}_L^2 + \mathbf{u}_R^2}{2}} \cdot \left(\mathrm{P}^+ + \mathrm{P}^- - 1\right)\bar{\rho}\bar{c} \tag{16c}$$

is borrowed from SLAU2. The rest of the parts are the same with AUSMPW+ or AUSMPW+–HLLI, resulting in AUSMPW+2 or AUSMPW+2–HLLI, respectively. We confirmed that in all the previous test cases this change did not affect the solutions. Let us mention that another all-speed version of AUSMPW+ is available in [87] for gasdynamics.

Figure 9 shows the pressure profiles in the first 20 cells at $t = 1$ of Problem 7. AUSMPW+2 preserved 13% of the initial amplitude, followed by AUSMPW+2–HLLI (13%). AUSMPW+ conserved slightly lower amplitude (12%), indicating the small but actual effect of the low Mach scaling introduced in AUSMPW+2 and AUSMPW+2–HLLI. In this problem, the SLAU2 showed the best performance (17%) and the Roe was the worst (11%).

Appendix 2: Analysis of SLAU2 for MHD

As conducted in [53], the SLAU2 for MHD behaviors at contact discontinuity and tangential discontinuity is compared with analytical solutions.

1. Contact discontinuity: $\rho_L \neq \rho_R, u_L = u_R = 0, v_L = v_R, w_L = w_R, B_{yL} = B_{yR}, B_{zL} = B_{zR}, p_L = p_R, B_x \neq 0$. Thus, referring to (1b),

$$\mathbf{Q} = \begin{bmatrix} \rho \\ \rho u \\ \rho v \\ \rho w \\ \rho E \\ B_x \\ B_y \\ B_z \end{bmatrix}, \quad \mathbf{F} = \begin{bmatrix} \rho u \\ \rho u^2 + p_{\mathrm{T}} - B_x^2 \\ \rho uv \quad - B_x B_y \\ \rho uw \quad - B_x B_z \\ \rho u H - B_x\,(\mathbf{u}\cdot\mathbf{B}) \\ 0 \\ uB_y - vB_x \\ uB_z - wB_x \end{bmatrix},$$

$$\mathbf{G} = \begin{bmatrix} \rho v \\ \rho vu \quad - B_y B_x \\ \rho v^2 + p_{\mathrm{T}} - B_y^2 \\ \rho vw \quad - B_y B_z \\ \rho v H - B_y\,(\mathbf{u}\cdot\mathbf{B}) \\ vB_x - uB_y \\ 0 \\ vB_z - wB_y \end{bmatrix}, \mathbf{H} = \begin{bmatrix} \rho w \\ \rho wu \quad - B_z B_x \\ \rho wv \quad - B_z B_y \\ \rho w^2 + p_{\mathrm{T}} - B_z^2 \\ \rho w H - B_z\,(\mathbf{u}\cdot\mathbf{B}) \\ wB_x - uB_z \\ wB_y - vB_z \\ 0 \end{bmatrix}, \tag{1b}$$

fluxes from left to right cells are: $F_{1,\mathrm{exact}} = \rho_L u_L = 0$; $F_{2,\mathrm{exact}} = p_{\mathrm{T}} - B_x^2$; $F_{3,\mathrm{exact}} = -B_x B_{y,L}$; $F_{4,\mathrm{exact}} = -B_x B_{z,L}$; $F_{5,\mathrm{exact}} = -B_x(v_L B_{y,L} + w_L B_{z,L})$; $(F_{6,\mathrm{exact}} = 0)$; $F_{7,\mathrm{exact}} = -v_L B_x$; $F_{8,\mathrm{exact}} = -w_L B_x$.

2. Tangential discontinuity: $\rho_L \neq \rho_R, u_L = u_R = 0, v_L \neq v_R, w_L \neq w_R, B_{yL} \neq B_{yR}, B_{zL} \neq B_{zR}, p_{\mathrm{T},L} = p_{\mathrm{T},R}, B_x = 0$. The corresponding analytical fluxes are: $F_{1,\mathrm{exact}} = \rho_L u_L = 0$; $F_{2,\mathrm{exact}} = p_{\mathrm{T}}$; $F_{3,\mathrm{exact}} = 0$; $F_{4,\mathrm{exact}} = 0$; $F_{5,\mathrm{exact}} = 0$; $(F_{6,\mathrm{exact}} = 0)$; $F_{7,\mathrm{exact}} = 0$; $F_{8,\mathrm{exact}} = 0$.

In the SLAU2,

$$(\dot{m})_{\mathrm{SLAU2}} = \frac{1}{2}\left\{\rho_L\left(u_L + \left|\bar{V}_n\right|^+\right) + \rho_R\left(u_R - \left|\bar{V}_n\right|^-\right) - \frac{\chi}{\bar{c}}\left(p_{\mathrm{T},R} - p_{\mathrm{T},L}\right)\right\} = 0 \tag{17}$$

and

$$(\tilde{p})_{\mathrm{SLAU2}} = \frac{p_{\mathrm{T},L} + p_{\mathrm{T},R}}{2} + \frac{\mathrm{P}^+ - \mathrm{P}^-}{2}\left(p_{\mathrm{T},L} - p_{\mathrm{T},R}\right) + \sqrt{\frac{\mathbf{u}_L^2 + \mathbf{u}_R^2}{2}} \cdot \left(\mathrm{P}^+ + \mathrm{P}^- - 1\right)\bar{\rho}\bar{c} = p_{\mathrm{T}} \tag{18}$$

at both discontinuities. Thus, the SLAU2 solutions are as follows:

1. Contact discontinuity

$$F_{1,\mathrm{SLAU2}} = 0 = F_{1,\mathrm{exact}}, \tag{19a}$$

$$F_{2,\mathrm{SLAU2}} = p_{\mathrm{T}} - B_x^2 = F_{2,\mathrm{exact}}, \tag{19b}$$

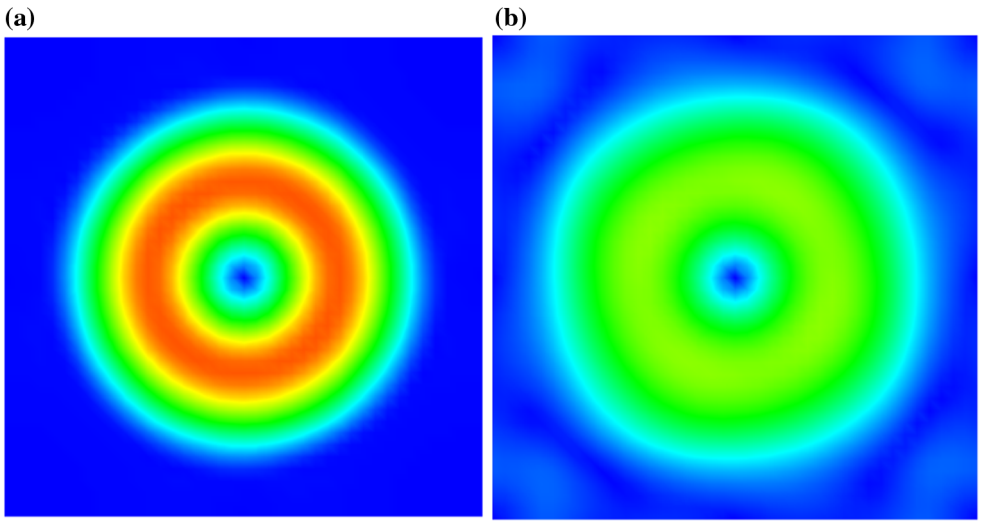

Fig. 10 Gresho vortex test solutions (Mach number contours, $0 \le M \le 0.01$). **a** SLAU2 and **b** Roe

$$F_{3,\mathrm{SLAU2}} = -B_x \frac{B_{y,L} + B_{y,R}}{2} = -B_x B_{y,L} = F_{3,\mathrm{exact}}, \tag{19c}$$

$$F_{4,\mathrm{SLAU2}} = -B_x \frac{B_{z,L} + B_{z,R}}{2} = -B_x B_{z,L} = F_{4,\mathrm{exact}}, \tag{19d}$$

$$\begin{aligned} F_{5,\mathrm{SLAU2}} &= -B_x \frac{v_L B_{z,L} + w_L B_{z,L} + v_R B_{z,R} + w_R B_{z,R}}{2}, \\ &= -B_x \left(v_L B_{z,L} + w_L B_{z,L} \right) = F_{5,\mathrm{exact}}, \end{aligned} \tag{19e}$$

since $\mathrm{P}^+ = \mathrm{P}^- = 0.5$ at $u = 0$.

$$F_{7,\,\mathrm{SLAU2}} = -v_L B_{\mathrm{x}} = F_{7,\,\mathrm{exact}}, \tag{19f}$$

$$F_{8,\,\mathrm{SLAU2}} = -w_L B_{\mathrm{x}} = F_{8,\,\mathrm{exact}}. \tag{19g}$$

Thus, the contact discontinuity is preserved by SLAU2.

2. Tangential discontinuity

Similarly,

$$F_{1,\,\mathrm{SLAU2}} = 0 = F_{1,\,\mathrm{exact}}, \tag{20a}$$

$$F_{2,\,\mathrm{SLAU2}} = p_{\mathrm{T}} = F_{2,\,\mathrm{exact}}, \tag{20b}$$

$$F_{3,\,\mathrm{SLAU2}} = 0 = F_{3,\,\mathrm{exact}}, \tag{20c}$$

$$F_{4,\,\mathrm{SLAU2}} = 0 = F_{4,\,\mathrm{exact}}, \tag{20d}$$

$$F_{5,\,\mathrm{SLAU2}} = 0 = F_{5,\,\mathrm{exact}}, \tag{20e}$$

$$F_{7,\,\mathrm{SLAU2}} = 0 = F_{7,\,\mathrm{exact}}, \tag{20f}$$

$$F_{8,\,\mathrm{SLAU2}} = 0 = F_{8,\,\mathrm{exact}}. \tag{20g}$$

Therefore, the tangential discontinuity is also proved to be conserved.

Appendix 3: Gresho Vortex

In order to confirm the efficacy of SLAU2 at a *low Mach number*, the Gresho vortex [91] is solved using SLAU2 (a three-wave solver *with* low Mach scaling) and Roe (a full-wave solver *without* low Mach scaling, as is the case also for the HLLI). The problem setup is as follows: A square domain of $[0, 1] \times [0, 1]$ is filled with 40×40 square cells, with the periodic boundary condition. The initial condition depends on the radius r from the vortex center, $(x_{\mathrm{c}}, y_{\mathrm{c}}) = (0.5, 0.5)$, i.e., $r = \sqrt{(x - x_{\mathrm{c}})^2 + (y - y_{\mathrm{c}})^2}$.

$$\rho = 1.0, \tag{21a}$$

$$p_0 = \frac{\rho}{\gamma M^2}, \tag{21b}$$

$$u_\theta = \begin{cases} 5r, & \text{if } 0 \le r \le 0.2, \\ 2 - 5r, & \text{if } 0.2 \le r \le 0.4, \\ 0, & \text{if } r \ge 0.4, \end{cases} \tag{21c}$$

$$p = \begin{cases} p_0 + 12.5r^2, & \text{if } 0 \le r \le 0.2, \\ p_0 + 12.5r^2 + 4\left(1 - 5r - \ln(0.2) + \ln(r)\right), & \text{if } 0.2 \le r \le 0.4, \\ p_0 - 2 + 4\ln(2), & \text{if } r \ge 0.4, \end{cases} \tag{21d}$$

where M is Mach number, $M = 0.01$, γ is the specific heat ratio, $\gamma = 1.4$, and u_θ is the angular velocity, converted to Cartesian velocity components as

$$u = -u_\theta \sin\theta = -u_\theta \frac{y - y_{\mathrm{c}}}{r}, \tag{22a}$$

$$v = -u_\theta \cos\theta = u_\theta \frac{x - x_{\mathrm{c}}}{r}, \tag{22b}$$

$$\theta = \arctan2\left(y - y_{\mathrm{c}}, x - x_{\mathrm{c}}\right). \tag{22c}$$

The computations are run for 20,000 steps with $\Delta t = 1 \times 10^{-4}$ (CFL ≈ 0.4), i.e., until $t = 2$. The Mach number contours are compared in Fig. 10. The SLAU2 clearly maintains the vortex structure, while it is smeared by the Roe-type Riemann solver.

Note that this problem is 2D gasdynamic. The MHD version of such a problem is left for future work, since multi-dimensional MHD involves divergence-free treatment which is beyond the scope of the present paper.

References

1. Esquivel, A., Raga, A.C., Cantó, J., Rodríguez-González, A., López-Cámara, D., Velázquez, P.F., De Colle, F.: Model of Mira's cometary head/tail entering the local bubble. Astrophys. J. **725**, 1466–1475 (2010). https://doi.org/10.1088/0004-637X/725/2/1466
2. Ohnishi, N., Kotake, K., Yamada, S.: Numerical analysis on standing accretion shock instability with neutrino heating in the supernova cores. Astrophys. J. **641**(2), 1018–1028 (2006). https://doi.org/10.1086/500554
3. Hanawa, T., Mikami, H., Matsumoto, T.: Improving shock irregularities based on the characteristics of the MHD equations. J. Comput. Phys. **227**, 7952–7976 (2008). https://doi.org/10.1016/j.jcp.2008.05.006
4. Poggie, J., Gaitonde, D.V.: Magnetic control of flow past a blunt body: numerical validation and exploration. Phys. Fluids **14**(5), 1720–1731 (2002). https://doi.org/10.1063/1.1465424
5. Burr, U., Barleon, L., Müller, U., Tsinober, A.: Turbulent transport of momentum and heat in magnetohydrodynamic rectangular duct flow with strong sidewall jets. J. Fluid Mech. **406**, 247–279 (2000). https://doi.org/10.1017/S0022112099007405
6. Godunov, S.K.: A finite difference method for the numerical computation of discontinuous solutions of the equations of fluid dynamics. Mat. Sb. Izd. Mosk. Mat. Obs. **47**(3), 271–306 (1959)
7. van Leer, B.: Towards the ultimate conservative difference scheme. V. A second-order sequel to Godunov's method. J. Comput. Phys. **32**(1), 101–136 (1979). https://doi.org/10.1016/0021-9991(79)90145-1
8. Colella, P.: A direct Eulerian MUSCL scheme for gas dynamics. SIAM J. Sci. Stat. Comput. **6**(1), 104–117 (1985). https://doi.org/10.1137/0906009
9. Colella, P., Woodward, P.R.: The Piecewise Parabolic Method (PPM) for gas-dynamical simulations. J. Comput. Phys. **54**, 174–201 (1984). https://doi.org/10.1016/0021-9991(84)90143-8
10. Roe, P.L.: Approximate Riemann solvers, parameter vectors, and difference schemes. J. Comput. Phys. **43**, 357–372 (1981). https://doi.org/10.1016/0021-9991(81)90128-5
11. Harten, A., Hyman, J.M.: Self adjusting grid methods for one-dimensional hyperbolic conservation laws. J. Comput. Phys. **50**, 235–269 (1983). https://doi.org/10.1016/0021-9991(83)90066-9
12. Harten, A., Lax, P.D., Van Leer, B.: On upstream differencing and Godunov-type schemes for hyperbolic conservation laws. SIAM Rev. **25**(1), 35–61 (1983). https://doi.org/10.1137/1025002
13. Einfeldt, B.: On Godunov-type methods for gas dynamics. SIAM J. Numer. Anal. **25**(2), 294–318 (1988). https://doi.org/10.1137/0725021
14. Einfeldt, B., Munz, C.D., Roe, P.L., Sjögreen, B.: On Godunov-type methods near low densities. J. Comput. Phys. **92**, 273–295 (1991). https://doi.org/10.1016/0021-9991(91)90211-3
15. Rusanov, V.V.: Calculation of interaction of non-steady shock waves with obstacles. J. Comput. Math. Phys. USSR **1**, 267–279 (1961)
16. Toro, E.F., Spruce, M., Speares, W.: Restoration of the contact surface in the HLL Riemann solver. Shock Waves **4**, 25–34 (1994). https://doi.org/10.1007/BF01414629
17. Batten, P., Clarke, N., Lambert, C., Causon, D.M.: On the choice of wavespeeds for the HLLC Riemann solver. SIAM J. Sci. Comput. **18**, 1553–1570 (1997). https://doi.org/10.1137/S1064827593260140
18. Osher, S., Solomon, F.: Upwind difference schemes for hyperbolic systems of conservation laws. Math. Comput. **38**(158), 339–374 (1982). https://doi.org/10.1090/S0025-5718-1982-0645656-0
19. Dumbser, M., Toro, E.F.: A simple extension of the Osher Riemann solver to non-conservative hyperbolic systems. J. Sci. Comput. **48**, 70–88 (2011). https://doi.org/10.1007/s10915-010-9400-3
20. Dumbser, M., Balsara, D.S.: A new efficient formulation of the HLLEM Riemann solver for general conservative and non-conservative hyperbolic systems. J. Comput. Phys. **304**, 275–319 (2016). https://doi.org/10.1016/j.jcp.2015.10.014
21. Brio, M., Wu, C.C.: An upwind differencing scheme for the equations of ideal magnetohydrodynamics. J. Comput. Phys. **75**, 400–422 (1988). https://doi.org/10.1016/0021-9991(88)90120-9
22. Ryu, D.S., Jones, T.W.: Numerical magnetohydrodynamics in astrophysics: algorithm and test for one-dimensional flow. Astrophys. J. **442**, 228–258 (1995). https://doi.org/10.1086/175437
23. Roe, P.L., Balsara, D.S.: Notes on the eigensystem of magnetohydrodynamics. SIAM J. Appl. Math. **56**, 57–67 (1996). https://doi.org/10.1137/S003613999427084X
24. Cargo, P., Gallice, G.: Roe matrices for ideal MHD and systematic construction of Roe matrices for systems of conservation laws. J. Comput. Phys. **136**, 446–466 (1997). https://doi.org/10.1006/jcph.1997.5773
25. Balsara, D.S.: Linearized formulation of the Riemann problem for adiabatic and isothermal magnetohydrodynamics. Astrophys. J. Suppl. **116**, 119–131 (1998). https://doi.org/10.1086/313092
26. Miyoshi, T., Kusano, K.: A multi-state HLL approximate Riemann solver for ideal magnetohydrodynamics. J. Comput. Phys. **208**, 315–344 (2005). https://doi.org/10.1016/j.jcp.2005.02.017
27. Gurski, K.F.: An HLLC-type approximate Riemann solver for ideal magnetohydrodynamics. SIAM J. Sci. Comput. **25**(6), 2165–2187 (2004). https://doi.org/10.1137/S1064827502407962
28. Li, S.: An HLLC Riemann solver for magnetohydrodynamics. J. Comput. Phys. **203**, 344–357 (2005). https://doi.org/10.1016/j.jcp.2004.08.020
29. Liou, M.S., Steffen Jr., C.J.: A new flux splitting scheme. J. Comput. Phys. **107**(1), 23–39 (1993). https://doi.org/10.1006/jcph.1993.1122
30. Liou, M.S.: A sequel to AUSM: AUSM+. J. Comput. Phys. **129**(2), 364–382 (1996). https://doi.org/10.1006/jcph.1996.0256
31. Kim, K.H., Kim, C., Rho, O.H.: Methods for the accurate computations of hypersonic flows: I. AUSMPW+ scheme. J. Comput. Phys. **174**, 38–80 (2001). https://doi.org/10.1006/jcph.2001.6873
32. Liou, M.-S.: A sequel to AUSM, part II: AUSM+-up for all speeds. J. Comput. Phys. **214**, 137–170 (2006). https://doi.org/10.1016/j.jcp.2005.09.020
33. Shima, E., Kitamura, K.: Parameter-free simple low-dissipation AUSM-family scheme for all speeds. AIAA J. **49**(8), 1693–1709 (2011). https://doi.org/10.2514/1.J050905
34. Kitamura, K., Shima, E.: Towards shock-stable and accurate hypersonic heating computations: a new pressure flux for AUSM-family schemes. J. Comput. Phys. **245**, 62–83 (2013). https://doi.org/10.1016/j.jcp.2013.02.046
35. Kitamura, K., Shima, E., Fujimoto, K., Wang, Z.J.: Performance of low-dissipation Euler fluxes and preconditioned LU-SGS at low

speeds. Commun. Comput. Phys. **10**(1), 90–119 (2011). https://doi.org/10.4208/cicp.041109.160910a
36. Weiss, J.M., Smith, W.A.: Preconditioning applied to variable and constant density flows. AIAA J. **33**(11), 2050–2057 (1995). https://doi.org/10.2514/3.12946
37. Li, X., Gu, C.: An all-speed Roe-type scheme and its asymptotic analysis of low Mach number behavior. J. Comput. Phys. **227**, 5144–5159 (2008). https://doi.org/10.1016/j.jcp.2008.01.037
38. Kitamura, K.: Assessment of SLAU2 and other flux functions with slope limiters in hypersonic shock-interaction heating. Comput. Fluids **129**, 134–145 (2016). https://doi.org/10.1016/j.compfluid.2016.02.006
39. Pandolfi, M., D'Ambrosio, D.: Numerical instabilities in upwind methods: analysis and cures for the "Carbuncle" phenomenon. J. Comput. Phys. **166**(2), 271–301 (2001). https://doi.org/10.1006/jcph.2000.6652
40. Kitamura, K., Shima, E., Roe, P.: Carbuncle phenomena and other shock anomalies in three dimensions. AIAA J. **50**(12), 2655–2669 (2012). https://doi.org/10.2514/1.J051227
41. Chauvat, Y., Moschetta, J.M., Gressier, J.: Shock wave numerical structure and the carbuncle phenomenon. Int. J. Numer. Methods Fluids **47**(8–9), 903–909 (2005). https://doi.org/10.1002/fld.916
42. Dumbser, M., Moschetta, J.M., Gressier, J.: A matrix stability analysis of the carbuncle phenomenon. J. Comput. Phys. **197**(2), 647–670 (2004). https://doi.org/10.1016/j.jcp.2003.12.013
43. Quirk, J.J.: A contribution to the great Riemann solver debate. Int. J. Numer. Methods Fluids **18**(6), 555–574 (1994). https://doi.org/10.1002/fld.1650180603
44. Kitamura, K., Roe, P., Ismail, F.: Evaluation of Euler fluxes for hypersonic flow computations. AIAA J. **47**, 44–53 (2009). https://doi.org/10.2514/1.33735
45. Barth, T.J.: Some notes on shock-resolving flux functions part 1: stationary characteristics. NASA TM-101087 (1989)
46. Hanayama, H., Takahashi, K., Tomisaka, K.: Generation of seed magnetic fields in primordial supernova remnants. ArXiv e-prints arXiv:0912.2686 (2009)
47. Balsara, D.S.: Total variation diminishing scheme for adiabatic and isothermal magnetohydrodynamics. Astrophys. J. Suppl. Ser. **116**, 133–153 (1998). https://doi.org/10.1086/313093
48. Stone, J.M., Gardiner, T.A., Teuben, P., Hawley, J.F., Simon, J.B.: ATHENA: a new code for astrophysical MHD. Astrophys. J. Suppl. Ser. **178**(1), 137–177 (2008). https://doi.org/10.1086/588755
49. Matsumoto, Y., Asahina, Y., Kudoh, Y., Kawashima, T., Matsumoto, J., Takahashi, H.R., Minoshima, T., Zenitani, S., Miyoshi, T., Matsumoto, R.: Magnetohydrodynamic simulation code CANS+: assessments and applications. ArXiv e-prints arXiv:1611.01775 (2016)
50. Tzeferacos, P., Fatenejad, M., Flocke, N., Graziani, C., Gregori, G., Lamb, D.Q., Lee, D., Meinecke, J., Scopatz, A., Weide, K.: FLASH MHD simulations of experiments that study shock-generated magnetic fields. High Energy Density Phys. **17**(Part A), 24–31 (2015). https://doi.org/10.1016/j.hedp.2014.11.003
51. Mignone, A., Bodo, G., Massaglia, S., Matsakos, T., Tesileanu, O., Zanni, C., Ferrari, A.: PLUTO: a numerical code for computational astrophysics. (2007) arXiv:astro-ph/0701854
52. Shen, Y., Zha, G., Huerta, M.A.: E-CUSP scheme for the equations of ideal magnetohydrodynamics with high order WENO scheme. J. Comput. Phys. **231**, 6233–6247 (2012). https://doi.org/10.1016/j.jcp.2012.04.015
53. Han, S.H., Lee, J.I., Kim, K.H.: Accurate and robust pressure weight advection upstream splitting method for magnetohydrodynamics equations. AIAA J. **47**(4), 970–981 (2009). https://doi.org/10.2514/1.39375
54. Xisto, C.M., Páscoa, J.C., Oliveira, P.J.: A pressure-based high resolution numerical method for resistive MHD. J. Comput. Phys. **275**, 323–345 (2014). https://doi.org/10.1016/j.jcp.2014.07.009
55. Kitamura, K., Hashimoto, A.: Reduced dissipation AUSM-family fluxes: HR-SLAU2 and HR-AUSM+-up for high resolution unsteady flow simulations. Comput. Fluids **126**, 41–57 (2016). https://doi.org/10.1016/j.compfluid.2015.11.014
56. Matsuyama, S.: Performance of all-speed AUSM-family schemes for DNS of low Mach number turbulent channel flow. Comput. Fluids **91**, 130–143 (2014). https://doi.org/10.1016/j.compfluid.2013.12.010
57. Batchelor, G.K.: The conditions for dynamical similarity of motions of a frictionless perfect-gas atmosphere. Q. J. R. Meteorol. Soc. **79**(340), 224–235 (1953). https://doi.org/10.1002/qj.49707934004
58. Ogura, Y., Phillips, N.: Scale analysis of deep and shallow convection in the atmosphere. J. Atmos. Sci. **19**, 173–179 (1962) https://doi.org/10.1175/1520-0469(1962)019<0173:SAODAS>2.0.CO;2
59. Gough, D.O.: The anelastic approximation for thermal convection. J. Atmos. Sci. **26**, 448–456 (1969). https://doi.org/10.1175/1520-0469(1969)026<0448:TAAFTC>2.0.CO;2
60. Hotta, H., Rempel, M., Yokoyama, T.: High-resolution calculations of the solar global convection with the reduced speed of sound technique. I. The structure of the convection and the magnetic field without the rotation. Astrophys. J. **786**, 24 (2014). https://doi.org/10.1088/0004-637X/786/1/24
61. Brown, B.P., Vasil, G.M., Zweibel, E.G.: Energy conservation and gravity waves in sound-proof treatments of stellar interiors. Part I. Anelastic approximations. Astrophys. J. **756**, 109 (2012). https://doi.org/10.1088/0004-637X/756/2/109
62. Vasil, G.M., Lecoanet, D., Brown, B.P., Wood, T.S., Zweibel, E.G.: Energy conservation and gravity waves in sound-proof treatments of stellar interiors. II. Lagrangian constrained analysis. Astrophys. J. **773**, 169 (2013). https://doi.org/10.1088/0004-637X/773/2/169
63. Rogers, T.M., Glatzmaier, G.A.: Angular momentum transport by gravity waves in the solar interior. Astrophys. J. **653**(1), 756–764 (2006). https://doi.org/10.1086/507259
64. Rogers, T.M., MacGregor, K.B.: On the interaction of internal gravity waves with a magnetic field—II. Convective forcing. Mon. Not. R. Astron. Soc. **410**(2), 946–962 (2011). https://doi.org/10.1111/j.1365-2966.2010.17493.x
65. MacGregor, K.B., Rogers, T.M.: Reflection and ducting of gravity waves inside the Sun. Sol. Phys. **270**(2), 417–436 (2011). https://doi.org/10.1007/s11207-011-9771-0
66. Brun, A.S., Miesch, M.S., Toomre, J.: Modeling the dynamical coupling of solar convection with the radiative interior. Astrophys. J. **742**, 79 (2011). https://doi.org/10.1088/0004-637X/742/2/79
67. Lantz, S.R.: Dynamical behavior of magnetic fields in a stratified, convecting fluid layer. Ph.D. Thesis, Cornell University (1992)
68. Braginsky, S.I., Roberts, P.H.: Equations governing convection in Earth's core and the geodynamo. Geophys. Astrophys. Fluid Dyn. **79**(1), 1–97 (1995). https://doi.org/10.1080/03091929508228992
69. ITER Physics Basis Editors et al.: ITER physics basis. Nucl. Fusion **39**, 2137 (1999). https://doi.org/10.1088/0029-5515/39/12/301
70. Loarte, A., Liu, F., Huijsmans, G.T.A., Kukushkin, A.S., Pitts, R.A.: MHD stability of the ITER pedestal and SOL plasma and its influence on the heat flux width. J. Nucl. Mater. **463**, 401–405 (2015). https://doi.org/10.1016/j.jnucmat.2014.11.122
71. Balsara, D.S.: Second-order-accurate schemes for magnetohydrodynamics with divergence-free reconstruction. Astrophys. J. Suppl. Ser. **151**, 149–184 (2004). https://doi.org/10.1086/381377
72. Balsara, D.S., Spicer, D.S.: A staggered Mesh algorithm using high order Godunov fluxes to ensure solenoidal magnetic fields in magnetohydrodynamics simulation. J. Comput. Phys. **149**, 270–292 (1999). https://doi.org/10.1006/jcph.1998.6153
73. Dedner, A., Kemm, F., Kröner, D., Munz, C.D., Schnitzer, T., Wesenberg, M.: Hyperbolic divergence cleaning for the MHD

equations. J. Comput. Phys. **175**, 645–673 (2002). https://doi.org/10.1006/jcph.2001.6961
74. Tóth, G.: The $\nabla \cdot \boldsymbol{B} = 0$ constraint in shock-capturing magnetohydrodynamics codes. J. Comput. Phys. **161**, 605–652 (2000). https://doi.org/10.1006/jcph.2000.6519
75. Powell, K.G., Roe, P.L., Linde, T., Gombosi, T.I., De Zeeuw, D.L.: A solution-adaptive upwind scheme for ideal magnetohydrodynamics. J. Comput. Phys. **154**, 284–309 (1999). https://doi.org/10.1006/jcph.1999.6299
76. Balsara, D.S.: Multidimensional HLLE Riemann solver; application to Euler and magnetohydrodynamic flows. J. Comput. Phys. **229**, 1970–1993 (2010). https://doi.org/10.1016/j.jcp.2009.11.018
77. Balsara, D.S.: A two-dimensional HLLC Riemann solver for conservation laws: application to Euler and magnetohydrodynamic flows. J. Comput. Phys. **231**, 7476–7503 (2012). https://doi.org/10.1016/j.jcp.2011.12.025
78. Balsara, D.S.: Multidimensional Riemann problem with self-similar internal structure, part I: application to hyperbolic conservation laws on structured meshes. J. Comput. Phys. **277**, 163–200 (2014). https://doi.org/10.1016/j.jcp.2014.07.053
79. Balsara, D.S., Nkonga, B.: Multidimensional Riemann problem with self-similar internal structure—part III—a multidimensional analogue of the HLLI Riemann solver for conservative hyperbolic systems. J. Comput. Phys. **346**, 25–48 (2017). https://doi.org/10.1016/j.jcp.2017.05.038
80. Balsara, D.S.: Self-adjusting, positivity preserving high order schemes for hydrodynamic and magnetohydrodynamics. J. Comput. Phys. **231**, 7504–7517 (2012). https://doi.org/10.1016/j.jcp.2012.01.032
81. Shima, E., Kitamura, K.: AUSM like expression of HLLC scheme and its extension to all speed scheme. In: 6th European Conference on Computational Fluid Dynamics (ECFD VI) Barcelona, Spain (2014)
82. Luo, H., Baum, J.D., Löhner, R.: Extension of Harten–Lax–van Leer scheme for flows at all speeds. AIAA J. **43**(6), 1160–1166 (2005). https://doi.org/10.2514/1.7567
83. Park, S.H., Lee, J.E., Kwon, J.H.: Preconditioned HLLE method for flows at all Mach numbers. AIAA J. **44**(11), 2645–2653 (2006). https://doi.org/10.2514/1.12176
84. Stix, M.: The Sun: An Introduction, 2nd edn. Astronomy and Astrophysics Library. Springer, Berlin (2002). ISBN 3-540-20741-4. https://doi.org/10.1007/978-3-642-56042-2
85. Huang, K., Wu, H., Yu, H., Yan, D.: Cures for numerical shock instability in HLLC solver. Int. J. Numer. Methods Fluids **65**(9), 1026–1038 (2011). https://doi.org/10.1002/fld.2217
86. Zha, G., Shen, Y., Huerta, M.: Rotated hybrid low diffusion ECUSP-HLL scheme and its applications to hypersonic flows. In: 20th AIAA Computational Fluid Dynamics Conference, AIAA Paper 2011-3545 (2011). https://doi.org/10.2514/6.2011-3545
87. Ihm, S.-W., Kim, C.: Computations of homogeneous-equilibrium two-phase flows with accurate and efficient shock-stable schemes. AIAA J. **46**(12), 3012–3037 (2008). https://doi.org/10.2514/1.35097
88. Dai, W., Woodward, P.R.: An approximate Riemann solver for ideal magnetohydrodynamics. J. Comput. Phys. **111**, 354–372 (1994). https://doi.org/10.1006/jcph.1994.1069
89. Pierce, A.D.: ACOUSTICS—An Introduction to Its Physical Principles and Applications, pp. 20–22. Acoustical Society of America, New York (1989)
90. Kitamura, K., Hashimoto, A., Murakami, K., Aoyama, T. and Nakamura, Y.: High resolution CFD/CAA hybrid analysis of supersonic jet interacting with walls. In: 37th AIAA Fluid Dynamics Conference and Exhibit, Miami, FL, AIAA Paper 2007-3871 (2007). https://doi.org/10.2514/6.2007-3871
91. Happenhofer, N., Grimm-Strele, H., Kupka, F., Löw-Baselli, B., Muthsam, H.: A low Mach number solver: enhancing applicability. J. Comput. Phys. **236**, 96–118 (2013). https://doi.org/10.1016/j.jcp.2012.11.002